

Electronic Supplementary Information

A novel covalent triazine-based frameworks as photocatalysts for the degradation of dyes under visible light irradiation

Yajing Du ^{a, b}, Haoqiang Ai ^a, Yun Liu ^c, and Hongzhi Liu ^{b*}

^a Shandong Institute of Advanced Technology, 250100, Jinan, China

^b International Center for Interdisciplinary Research and Innovation of Silsesquioxane Science; Key Laboratory of Special Functional Aggregated Materials, Ministry of Education, School of Chemistry and Chemical Engineering, Shandong University, Jinan 250100, P. R. China

^cInstitute of High Performance Computing (IHPC), Agency for Science, Technology and Research (A*STAR), 1 Fusionopolis Way, #16-16 Connexis, Singapore 138632, Republic of Singapore

Table of Contents

Experimental Section

Table S1. Elemental analysis of TAs and PTCTFs.

Table S2. Porosity data of PTCTFs.

Table S3. Comparison of the photocatalytic performance of different related catalysts for degradation of CR, RB, MB and MO.

Table S4. Physical and chemical properties of dyes.

Table S5. Detected intermediates of RB degradation by 3Ph-CTF using HPLC-MS.

Table S6. Detected intermediates of CR degradation by 3Ph-CTF using HPLC-MS.

Table S7. Detected intermediates of MB degradation by 3Ph-CTF using HPLC-MS.

Table S8. Detected intermediates of MO degradation by 3Ph-CTF using HPLC-MS.

Fig. S1. FE-SEM images of 2Ph_{mix}-CTF.

Fig. S2. FE-SEM images of 2Th_{mix}-CTF.

Fig. S3. FE-SEM images of 3Th-CTF.

Fig. S4. HR-TEM images of 2Ph_{mix}-CTF.

Fig. S5. HR-TEM images of 2Th_{mix}-CTF.

Fig. S6. HR-TEM images of 3Th-CTF.

Fig. S7. TGA curves of PTCTFs.

Fig. S8. Photographs of the changes of a) RB b) MB c) MO and d) CR solutions with time in the presence of 3Ph-CTF, 3Th-CTF, 2Ph_{mix}-CTF, and 2Th_{mix}-CTF outside under natural light (standstill state).

Fig. S9. The MS spectra of the photodegradation products of RB at different photodegradation times: (a) 5 min, (b) 15 min, and (c) 45 min.

Fig. S10. The MS spectra of the photodegradation products of CR at different photodegradation times: (a) 5 min, (b) 15 min, and (c) 40 min.

Fig. S11. The MS spectra of the photodegradation products of MB at different photodegradation times: (a) 25 min, (b) 60 min, and (c) 160 min.

Fig. S12. The MS spectra of the photodegradation products of MO at different photodegradation times: (a) 40 min, (b) 70 min, and (c) 160 min.

Fig. S13. Valence band UPS cutoff spectra of PTCTFs.

Fig. S14. The plots of $(\alpha h\nu)^{1/2}$ versus photon energy ($h\nu$) for CTFs.

Fig. S15. The Kohn-Sham orbitals of HOMO and LUMO of CTFs.

Fig. S16. The energy band structures of 3Ph-CTF and 3Th-CTF calculated by DFT.

Scheme S1. Degradation pathway of RB by 3Ph-CTF based on degradation intermediates detected by LC-MS.

Scheme S2. Degradation pathway of CR by 3Ph-CTF based on degradation intermediates detected by LC-MS.

Scheme S3. Degradation pathway of MB by 3Ph-CTF based on degradation intermediates detected by LC-MS.

Scheme S4. Degradation pathway of MO by 3Ph-CTF based on degradation intermediates detected by LC-MS.

References

Experimental Section

Materials

Unless otherwise mentioned, materials were obtained from commercial suppliers and used without further purification.

Characterization

Fourier-transform infrared (FTIR) spectra were recorded with a Bruker Tensor-27 infrared spectrophotometer with a disc of KBr from 4000 to 400 cm^{-1} . Solid-state ^{13}C CP/MAS NMR spectra were carried out on a Bruker Avance-500 NMR spectrometer operating under a magnetic field strength of 9.4 T. The resonance frequency at this field strength was 125 MHz for ^{13}C NMR. A chemagnetics of 5 mm triple-resonance MAS probe was used to acquire ^{13}C spectra. The ^{13}C chemical shifts were referenced externally via the resonance of tetramethylsilane (TMS) of 0 ppm. Elemental analysis was performed by using an Elementarvario EL III elemental analyzer. Powder X-ray diffraction (PXRD) were performed on a Rigaku D/MAX 2550 diffractometer using Cu- $K\alpha$ radiation at 40 kV and 200 mA with a scan rate of $10^\circ \text{ min}^{-1}$. Thermal gravimetric analysis (TGA) was measured on a Mettler-Toledo TGA/DSC TGA system with heating rate of $10^\circ \text{ C min}^{-1}$ from room temperature to 800° C in nitrogen atmosphere. Field-emission scanning electron microscopy (FE-SEM) experiments were recorded with a HITACHI S4800 spectrometer. UV-vis absorption spectra were collected on a TU-1901 double beam UV-vis spectrophotometer. The high-resolution transmission electron microscopy (HR-TEM) experiments were characterized by using a JEM 2100 electron microscope (JEOL, Japan) with an acceleration voltage of 200 kV. The luminescence excitation spectra and emission spectra were measured on Hitachi F-4500 fluorescence spectrophotometer equipment. UV-vis absorption spectra were collected on an Agilent Cary 5000 UV-Vis-NIR Spectrophotometer. XPS analysis of the solid samples was performed using ThermoFisher ESCALAB 250 spectrometer with monochromatized Al $K\alpha$ radiation under ultrahigh vacuum ($<10^{-7}$ Pa). The binding energies were calibrated using C1s peak (284.6 eV) as a reference. UPS measurements were performed using Thermo Escalab 250XI PHI5000 Versa Probe III instrument with an unfiltered He I (21.22 eV) gas discharge lamp and a gold (Au) calibration. A typical UPS spectrum usually has two intersections with baseline, from which the width of binding energy (ΔE) is determined. The width value of He I UPS spectra (21.22 eV) is used as the standard. Nitrogen sorption isotherm measurements were performed by using a Micro Meritics surface area and pore size analyzer. The samples were degassed at 150° C for 12 h prior to measurement. A sample of ca. 100 mg and UHP-grade nitrogen (99.999%) gas source were used in the nitrogen sorption measurements and collected with a Quantachrome Quadrasorb apparatus. Brunauer-Emmet-Teller (BET) surface areas were evaluated over a P/P_0 range from 0.01 to 0.20. Nonlocal density functional theory (NL-DFT) pore-size distributions were confirmed by using the carbon/slit-cylindrical pore mode of the Quadrawin software. (Surface area calculated from N_2 adsorption isotherm using the BET method; Microporous surface area calculated from N_2 adsorption isotherm using t-plot method; Total pore volume calculated at $P/P_0 = 0.99$; Micropore volume derived using the t-plot method.) Radicals ($\cdot\text{O}_2^-$ and $\text{OH}\cdot$) were detected by electron paramagnetic resonance (EPR, EMX PLUS, Bruker, Germany) spectroscopy with 100 mM of DMPO as the spin trapping agent. The intermediates of dye degradation were analyzed by high performance liquid chromatography mass spectrometry (HPLC-MS) (Thermo Scientific Q Exactive) with a C18 column (2.1 mm \times 100 mm, 2.6 μm). The intermediates of RB and MB were measured in positive electrospray ionization (ESI) mode, while the intermediates of CR and MO were analyzed in negative ESI mode. The injection volume was 10 μL . The column temperature was 25° C . The flow rate was 0.2 mL/min. The mobile phase was consisted by A (acetonitrile) and B (0.1% formic acid-water); moreover, gradient elution was used in following method.

RB: 20%A-80%B (0-12 min), 75%A-25%B (12-15 min), and 20%A-80%B (15-23 min).

MB: 18%A-82%B (0-12 min), 72%A-28%B (12-15 min), and 18%A-82%B (15-23 min).

CR: 5%A-95%B (0-12 min), 80%A-20%B (12-14 min), and 5%A-95% (14-20 min).

MO: 5%A-95%B (0-10 min), 70%A-30%B (10-14 min), and 5%A-95% (14-20 min).

Photoelectrochemical measurements

The transient photocurrent response and electrochemical impedance measurements were performed using a CHI760E electrochemical workstation with a standard three-electrode system. The working electrode was prepared as follows: 10 mg CTFs was dispersed in a mixture of 5 % Nafion solution (50 μ L) and isopropanol (1 mL) and ultrasonicated for 30 min to form a uniform suspension. Then, 150 μ L of suspension was dip-coated on the 1 cm \times 0.8 cm ITO glass and dried overnight at room temperature. The as-prepared electrode, platinum electrode and Ag/AgCl electrode were acted as working electrode, counter electrode, and reference electrode, respectively. The electrolyte was 0.5 M Na₂SO₄ aqueous solution, and the light source is a 300 W Xe-lamp.

General Synthesis Procedure for TAs

All trimerization reactions were carried out in a dried three-necked flask equipped with a magnetic stirrer, using chloroform as the solvent. The molar ratio of trifluoromethanesulfonic acid (CF₃SO₃H) to the cyano group was set to 3:1. For the products 2Ph_{mix}-TA and 2Th_{mix}-TA, the monomer ratios of 4-bromobenzonitrile and 5-bromothiophene-2-carbonitrile were 2: 1 and 2: 1, respectively.

Synthesis of 3Ph-TA. A dried 50 mL flask was equipped with a magnetic stirrer and dry chloroform (20 mL) under argon. After the solvent had been cooled to 0 °C in an ice bath, CF₃SO₃H (4.50 g, 30 mmol) was added carefully under vigorous stirring. Then, 4-bromobenzonitrile (1.82 g, 10 mmol) was added in small portions. The reaction mixture was stirred at 0 °C for 1 h and afterward for an additional 36 h at room temperature. After 50 mL of water had been added, a white precipitate was formed. Being stirred for an additional 3 h, the suspension was filtered, washed successively with water (50 mL), ethanol (50 mL) and diethyl ether (50 mL). The samples were obtained as a white powder and dried under vacuum at 75 °C overnight (yield: 1.11 g, 61 %).

Synthesis of 2Ph_{mix}-TA. 4-bromobenzonitrile (1.82 g, 10 mmol), 5-bromothiophene-2-carbonitrile (0.94 g, 5 mmol), and CF₃SO₃H (6.75 g, 45 mmol) were used in this cyclotrimerization. 2Ph_{mix}-TA was obtained as an off-white powder (yield: 1.60 g, 58 %).

Synthesis of 2Th_{mix}-TA. 4-bromobenzonitrile (0.91 g, 5 mmol), 5-bromothiophene-2-carbonitrile (1.88 g, 10 mmol), and CF₃SO₃H (6.75 g, 45 mmol) were used in this cyclotrimerization. 2Th_{mix}-TA was obtained as a pale-yellow powder (yield: 1.48 g, 53 %).

Synthesis of 3Th-TA. 5-bromothiophene-2-carbonitrile (1.88 g, 10 mmol), and CF₃SO₃H (4.50 g, 30 mmol) were used in this cyclotrimerization. 3Th-TA was obtained as a pale-yellow powder (yield: 0.88 g, 47 %).

Synthesis of PTCTFs

Synthesis of 3Ph-CTF. The synthesis of 3Ph-CTF gives a representative example for the experimental procedure. All Suzuki reactions were carried out in a three-necked flask equipped with a magnetic stirrer and under N₂ atmosphere. A 100 mL oven-dried flask was charged with 3Ph-TA (1.09 g, 2 mmol), Pd[P(C₆H₅)₃]₄ (0.28 g, 0.24 mmol), and DMF (45 mL) under N₂ atmosphere. After stirring evenly, K₂CO₃ (2.0 M in water, 10 mL) and 1,4-phenylenebisboronic acid (0.74 g, 4.5 mmol, in 10 mL methanol) were then added. The mixture was slowly heated to 135 °C and stirred for 20 h under reflux. At the end of the reaction, the suspension reaction system was cooled to room temperature and poured into water (about 200 mL). After that, the product was precipitated, filtered, and sequentially washed with successive water, dichloromethane, and methanol. After the operations, 3Ph-CTF was afforded as a gray powder (yield: 0.71 g, 84 %).

Synthesis of 2Ph_{mix}-CTF. 2Ph_{mix}-TA (1.10 g), Pd[P(C₆H₅)₃]₄ (0.28 g, 0.24 mmol), DMF (45 mL), K₂CO₃ (2.0 M in water, 10 mL) and 1,4-phenylenebisboronic acid (0.74 g, 4.5 mmol, in 10 mL methanol) were used in this

polymerization. 2Ph_{mix}-CTF was obtained as a yellow powder (yield: 0.74 g, 86%).

Synthesis of 2Th_{mix}-CTF. 2Th_{mix}-TA (1.12 g), Pd[P(C₆H₅)₃]₄ (0.28 g, 0.24 mmol), DMF (45 mL), K₂CO₃ (2.0 M in water, 10 mL) and 1,4-phenylenebisboronic acid (0.74 g, 4.5 mmol, in 10 mL methanol) were used in this polymerization. 2Th_{mix}-CTF was obtained as a yellow-green powder (yield: 0.70 g, 81%).

Synthesis of 3Th-CTF. 3Th-TA (1.13 g), Pd[P(C₆H₅)₃]₄ (0.28 g, 0.24 mmol), DMF (45 mL), K₂CO₃ (2.0 M in water, 10 mL) and 1,4-phenylenebisboronic acid (0.74 g, 4.5 mmol, in 10 mL methanol) were used in this polymerization. 3Th-CTF was obtained as a brown-yellow powder (yield: 0.77 g, 88%).

Photodegradation Experiments

All the photodegradation experiments were carried out in 15 ml of dye solutions with different concentrations at room temperature, the concentrations of PTCTFs being the same, *ie* 0.2 g L⁻¹. The dye solutions were prepared by dissolving the corresponding dyes into deionized water. A UV-vis spectrophotometer was employed to record the changes of the intensity of the maximum absorption wavelength of RB (554 nm), CR (497 nm), MB (665 nm), and MO (464 nm) before and after the photodegradation experiments.

At the same time, to evaluate the degradation ability more accurately and exclude the influence of adsorption, we further conducted desorption experiments for each set of dye degradation experiments and analyzed the desorbed substances. After degrading and adsorbing for a certain period, PTCTFs were separated from the solutions by filtration, and then washed repeatedly many times with methanol until the detergent was colorless. The filtrates were then mixed, transferred to a volumetric flask, and diluted with methanol to volume. Similarly, UV-vis spectrophotometer was used to detect the concentrations of the desorbed dyes. In methanol, the maximum absorption wavelengths of RB, CR, MB, and MO are 545, 497, 663 and 421 nm. Before the photodegradation experiments, the relationships between absorbance and concentration of four dyes both in water and methanol were established by using UV-vis spectrophotometer. All photocatalytic experiments were quantitatively analyzed by the above steps.

Photocatalytic activity measurements. The photocatalytic activity of PTCTFs was tested under ultraviolet light irradiation in the laboratory. Due to the difference in absorptivity, the concentration of RB and CR aqueous solutions prepared for degradation experiment is 20 ppm, while that of MB and MO is 10 ppm.

Degradation experiments under natural light. Degradation experiments under natural light were stirred for two days. The controlled experiments were performed in the dark, other conditions being equal. The static degradation experiments of four dyes with gradient concentrations were carried out by exposure to outdoor natural light, and recorded regularly with photos.

Mechanism exploration experiments. The mechanism exploration experiments were carried out according to the above steps with the addition of scavenger (1 mmol L⁻¹).

Determination of degradation intermediates. Typically, 3Ph-CTF (3 mg) were dispersed into dye solution (15 mL), and the mixture was irradiated under a visible light (300 W Xe lamp). 4 mL of the solution was collected at selected irradiation times and centrifuged to obtain clear solutions. HPLC-MS was used to analyze the intermediate products of dye degradation. The concentration of the dye solution and the different intervals are shown below.

RB (20 ppm): 5 min, 15 min, 45 min.

MB (10 ppm): 25 min, 60 min, 16 min.

CR (20 ppm): 5 min, 15 min, 40 min.

MO (10 ppm): 40 min, 70 min, 160 min.

Photocatalytic regeneration experiments. Conditions: C₀=20 ppm, V=10 mL, M_{PTCTF}=2 mg, time = 1 h.

After the photodegradation experiment, the PTCTFs were filtered and collected, washed several times with hot methanol. Then the regenerated materials were dried under vacuum for 10 h at 80 °C and used directly in the next cycle.

Kubelka-Munk equation: $F(R_{\infty}) = [(1-R_{\infty})^2/(2R_{\infty})]$

$$\alpha h\nu = A (h\nu - E_g)^{n/2} \dots \dots \dots (4)$$

where α , $h\nu$, and A represent the absorption coefficient, the discrete photon energy, and the proportionality constant, respectively, and n depends on the form of the optical transition in the photocatalyst (with direct transitions $n = 1$, indirect transitions $n = 4$).

Computational methods

The density-functional-theory (DFT) calculations¹ were carried out with the Vienna *Ab initio* Simulation Package² to further understand the photocatalytic properties of the CTFs. The projector augmented wave pseudo-potentials method³ and the generalized gradient approximation in the form of Perdew–Burke–Ernzerhof (PBE)⁴ were applied. The cutoff energy for the plane-wave basis was set to 450 eV. The convergence criteria for energy and force were set to 10^{-5} eV and 0.01 eV/Å, respectively. The structures were fully relaxed with the Γ -centered Monkhorst-Pack⁵ k -point sampling which was set as $2 \times 2 \times 6$.

Table S1. Elemental analysis of TAs and PTCTFs.

Sample	Chemical formula or		N (%)	C (%)	H (%)	S (%)
	Theoretical molar ratio of	Si: O: C: H: N: S				
3Ph-TA	C ₂₁ H ₁₂ Br ₃ N ₃	Exp %	7.52	46.27	2.14	0.10
		Theo %	7.70	46.19	2.22	0
2Ph _{mix} -TA	C ₁₉ H ₁₀ Br ₃ N ₃ S	Exp %	7.44	41.52	1.87	5.73
		Theo %	7.61	41.34	1.83	5.81
2Th _{mix} -TA	C ₁₇ H ₈ Br ₃ N ₃ S ₂	Exp %	7.41	36.32	1.47	11.98
		Theo %	7.53	36.58	1.44	11.49
3Th-TA	C ₁₅ H ₆ Br ₃ N ₃ S ₃	Exp %	7.29	32.34	1.25	16.65
		Theo %	7.45	31.94	1.07	17.05
3Ph-CTF	2: 3: 18: 12: 2: 0	Exp %	8.66	80.58	4.67	0
		Theo %	9.99	85.69	4.31	0
2Ph _{mix} -CTF	6: 9: 50: 32: 6: 2	Exp %	8.23	75.55	4.40	5.99
		Theo %	9.85	78.85	3.78	7.52
2Th _{mix} -CTF	6: 9: 46: 28: 6: 4	Exp %	8.21	69.59	3.79	13.07
		Theo %	9.72	72.20	3.26	14.82
3Th-CTF	2: 3: 14: 8: 2: 2	Exp %	8.45	64.19	3.13	19.38
		Theo %	9.58	59.99	2.52	20.02

Exp % = Experimental Value

Theo % = Theoretical Value

Table S2. Porosity data of PTCTFs.

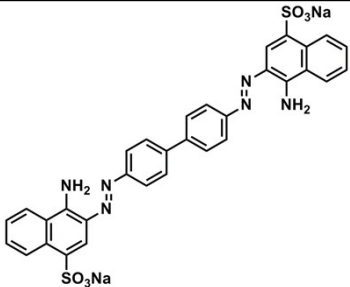
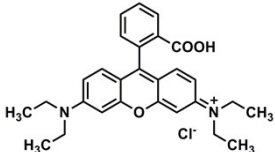
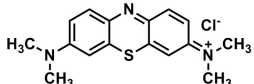
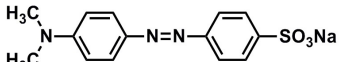
Sample	BET Surface Area (m ² g ⁻¹)	Mean Pore Diameter (nm)	Total Pore Volume (m ³ g ⁻¹)
3Ph-CTF	34	21.7	0.18
2Ph _{mix} -CTF	60	11.3	0.17
2Th _{mix} -CTF	68	12.6	0.21
3Th-CTF	46	24.8	0.28

Table S3. Comparison of the photocatalytic performances of different related catalysts for degradation of CR, RB, MB, and MO.

Photocatalyst and their Concentration (mg mL ⁻¹)		Dye	Concentration of the dye	$t_{1/2}$ (min) or k (min ⁻¹)	Removal Efficiency η (min)	Energy source	Ref.
Ag ₃ PO ₄	1.25 (pH=9)	CR	7.5×10 ⁻⁵ M (52 ppm)		91 % (18)	visible light	6
Ag ₃ PO ₄	1.25 (pH=9)	MO	7.5×10 ⁻⁵ M (25 ppm)		92 % (42)	visible light	6
[Cu ₂ (bix)(sdc) ₂] _n	0.40 (30% H ₂ O ₂)	MO	10 ppm		85 % (300)	visible light	7
[Cu ₂ (bix)(sdc) ₂] _n	0.40 (30% H ₂ O ₂)	MB	10 ppm		91 % (90)	visible light	7
[Cu ₂ (bix)(sdc) ₂] _n	0.40 (30% H ₂ O ₂)	RB	10 ppm		84 % (180)	visible light	7
ZnAl ₂ O ₄	1.00	CR	15 ppm	0.033 min ⁻¹	98 % (80)	mercury lamp	8
ZnAl ₂ O ₄	1.00	MO	15 ppm	0.032 min ⁻¹	97 % (90)	mercury lamp	8
Graphene-Cu-Co ₃ O ₄	0.30	CR	Dye wastewater: total nitrogen = 45 mg/L, total phosphorus = 2.5 mg/L, and color = 1000 unit	3.01 min 0.23 min ⁻¹	99 % (15)	visible light	9
Graphene-Cu-Co ₃ O ₄	0.30	MO		1.71 min 0.41 min ⁻¹	99 % (15)	visible light	9
MNP@TiO ₂ /WO ₃	5.00	CR	50 ppm	0.049 min ⁻¹	99 % (60)	solar light	10
MNP@TiO ₂ /WO ₃	5.00	MB	50 ppm	0.1677 h ⁻¹	99 % (12 h)	solar light	10
MNP@TiO ₂ /WO ₃	5.00	MO	10 ppm	0.1557 h ⁻¹	99 % (11 h)	solar light	10
POD (HCl 0.5 mol/L)	2.50	MO	25 ppm		75 % (70)	A 250-W medium-pressure Hg lamp	11
	2.50	MB	25 ppm		65 % (300)		11
Ni doped CdS nanoparticles	0.60	MB	20 ppm	1.18 min ⁻¹	91 % (75)	sunlight	12
	0.60	MO	20 ppm	1.22 min ⁻¹	94 % (75)	sunlight	12
ACN2	1.25	MB	6.67×10 ⁻⁷ M (0.2 ppm)	0.11 min ⁻¹	93 % (25)	artificial solar light	13
ACN2	1.25	MO	6.67×10 ⁻⁷ M (0.2 ppm)	0.07 min ⁻¹	84 % (25)	artificial solar light	13
Cu ₂ O/MoS ₂ -12	0.20	MO	20 ppm	0.084 min ⁻¹	90 % (30)	visible light	14
POP-1	1.00	RB	10 ppm	11 min 0.067 min ⁻¹	> 99 (45)	visible light	15
POP-1	1.00	MB	10 ppm	18 min 0.044 min ⁻¹	> 99 % (30)	visible light	15

POP-1	1.00	CR	20 ppm	28 min 0.022 min ⁻¹	90 % (45)	visible light	15
POP-1	1.00	MO	20 ppm	71 min 0.007 min ⁻¹	91 % (150)	visible light	15
POP-2	1.00	RB	10 ppm	16 min 0.039 min ⁻¹	90 % (120)	visible light	15
POP-2	1.00	MB	10 ppm	28 min 0.025 min ⁻¹	96 % (75)	visible light	15
POP-2	1.00	CR	20 ppm	22 min 0.032 min ⁻¹	67 % (75)	visible light	15
POP-2	1.00	MO	20 ppm	N.A.	2 % (160)	visible light	15
COP-NT	1.00 (H ₂ O ₂ : 0.10 M, pH=7)	MO	5.0 × 10 ⁻⁵ M (16.4 ppm)	459 min 0.002 min ⁻¹	67 % (12 h)	visible light	16
3Ph-CTF	0.20	CR	20	6.8 min 0.115 min ⁻¹	98 % (30)	UV light	This work
3Ph-CTF	0.20	RB	20	9.7 min 0.086 min ⁻¹	> 99 % (30)	UV light	This work
3Ph-CTF	0.20	MB	10	26.0 min 0.030 min ⁻¹	95 % (100)	UV light	This work
3Ph-CTF	0.20	MO	10	43.0 min 0.024 min ⁻¹	93 % (120)	UV light	This work
3Th-CTF	0.20	CR	20	7.4 min 0.074 min ⁻¹	91 % (30)	UV light	This work
3Th-CTF	0.20	RB	20	13.3 min 0.063 min ⁻¹	95 % (45)	UV light	This work
3Th-CTF	0.20	MB	10	148.5 min 0.004 min ⁻¹	75 % (300)	UV light	This work
3Th-CTF	0.20	MO	10	134.3 min 0.006 min ⁻¹	83 % (260)	UV light	This work

Table S4. Physical and chemical properties of dyes.

Dyes	Structure	Molecular weight (g mol ⁻¹)	Nature	UV Adsorption (nm)
CR		696	anion	497
RB		478	cation	554
MB		320	cation	665
MO		327	anion	466

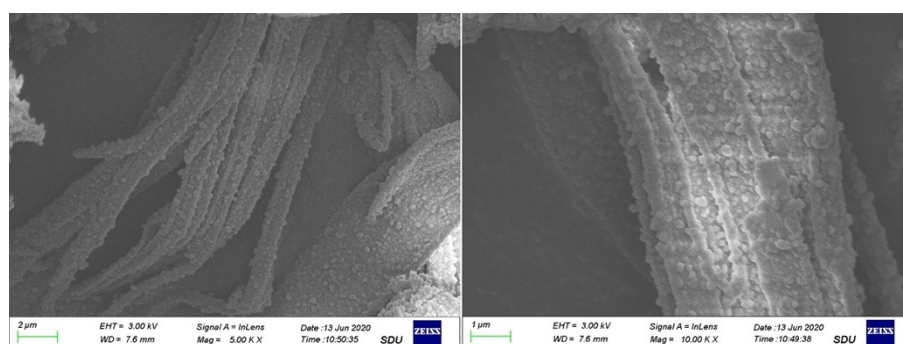


Fig. S1. FE-SEM images of 2Ph_{mix}-CTF.

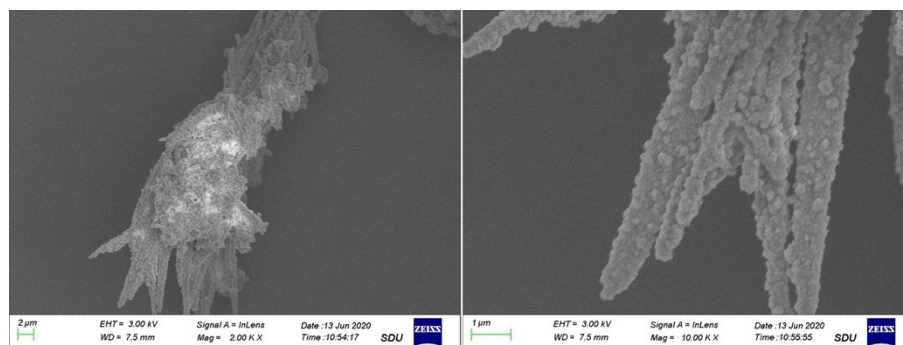


Fig. S2. FE-SEM images of 2Th_{mix}-CTF.

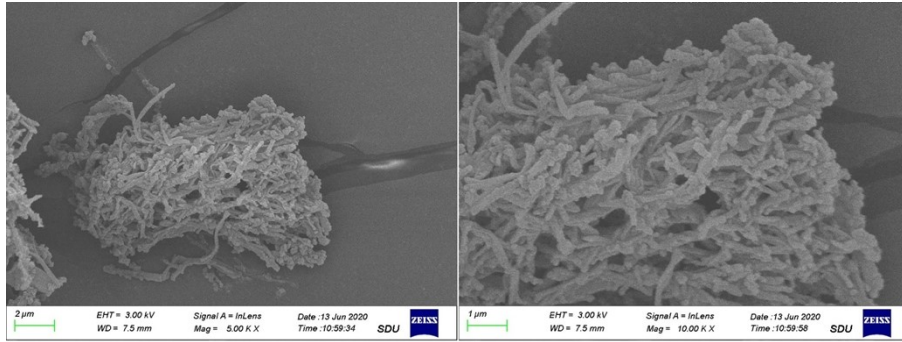


Fig. S3. FE-SEM images of 3Th-CTF.

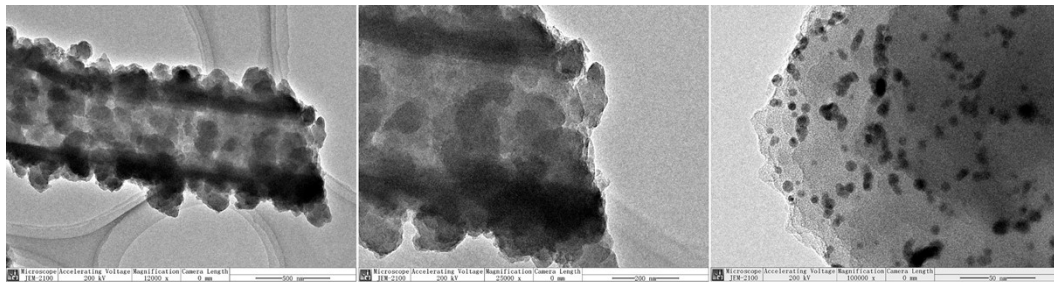


Fig. S4. HR-TEM images of 2Ph_{mix}-CTF.

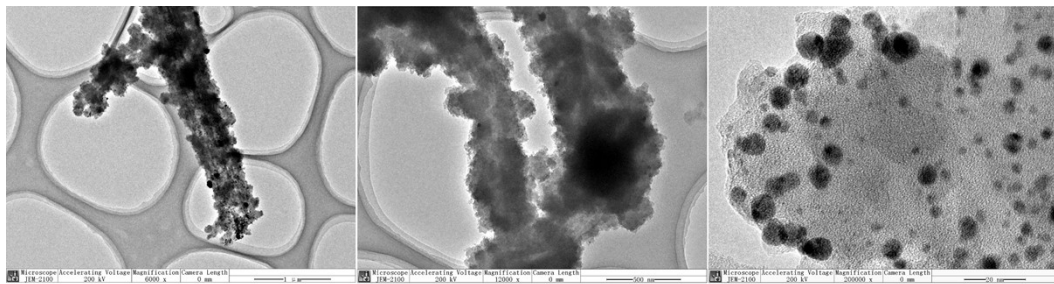


Fig. S5. HR-TEM images of 2Th_{mix}-CTF.

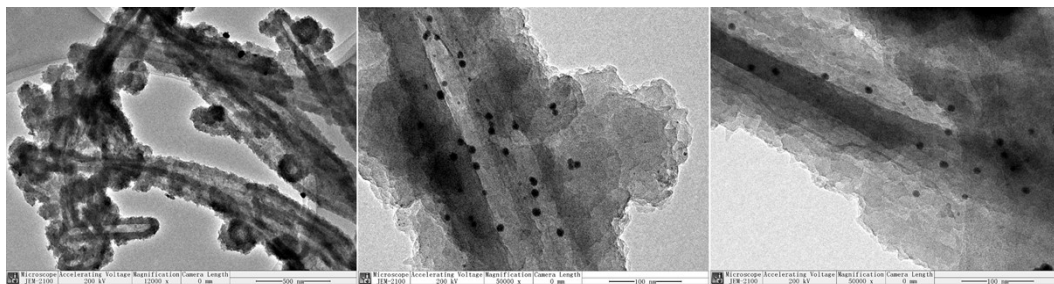


Fig. S6. HR-TEM images of 3Th-CTF.

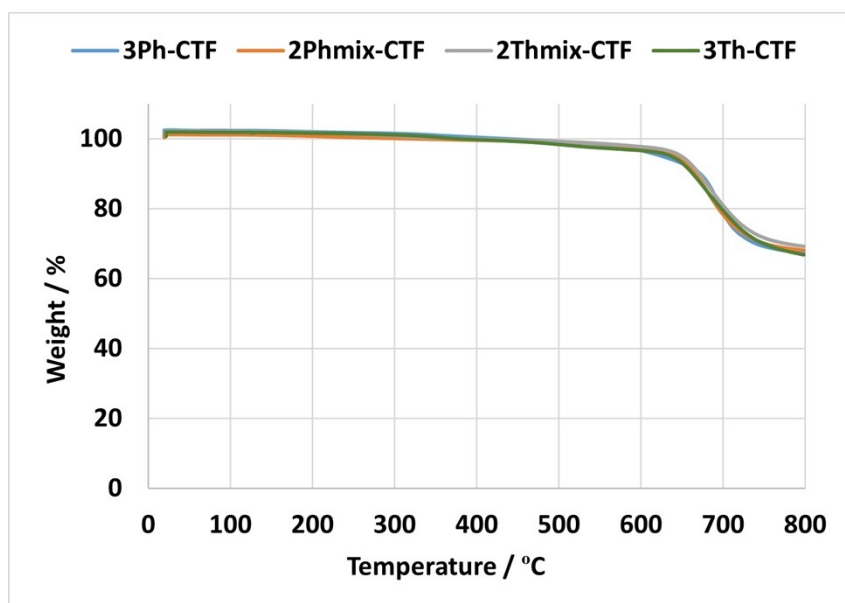


Fig. S7. TGA curves of PTCTFs.



Fig. S8. Photographs of the changes of a) RB b) MB c) MO and d) CR solutions with time in the presence of 3Ph-CTF, 3Th-CTF, 2Ph_{mix}-CTF, and 2Th_{mix}-CTF outside under natural light (standstill state).

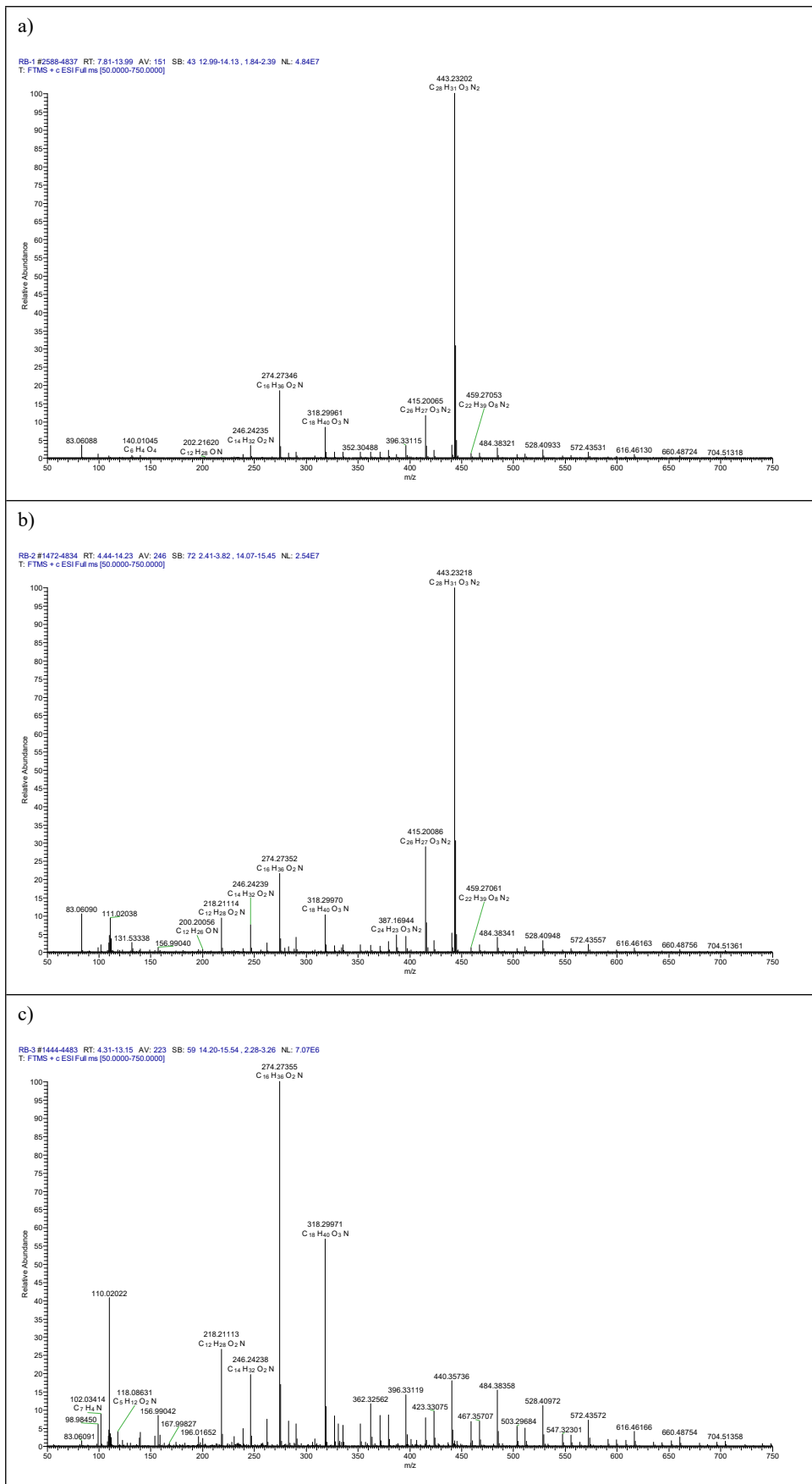
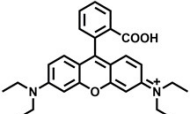
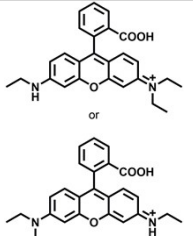
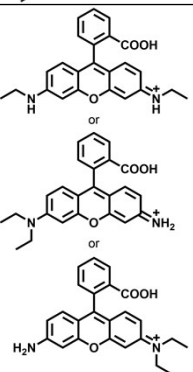
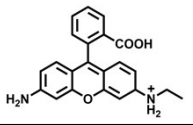
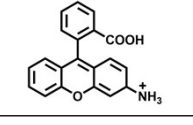
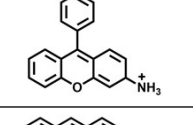
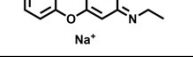
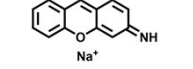
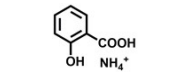
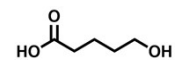
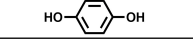
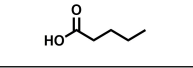
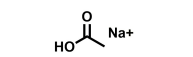


Fig. S9. The MS spectra of the photodegradation products of RB at different photodegradation times: (a) 5 min, (b) 15 min, and (c) 45 min.

Table S5. Detected intermediates of RB degradation by 3Ph-CTF using HPLC-MS.

Compounds	Chemical structure	Molecular formula	Molecular weight	m/z
RB		$C_{28}H_{31}N_2O_3^+$	443	443
1		$C_{26}H_{27}N_2O_3^+$	415	415
2		$C_{24}H_{23}N_2O_3^+$	387	387
3		$C_{22}H_{21}N_2O_3^+$	361	361
4		$C_{20}H_{16}NO_3^+$	318	318
5		$C_{19}H_{16}NO^+$	274	274
6		$C_{15}H_{13}NNaO^+$	246	246
7		$C_{13}H_9NNaO^+$	218	218
8		$C_7H_{10}NO_3^+$	156	156
9		$C_5H_{10}O_3$	118	118
10		$C_6H_6O_2$	110	110
11		$C_5H_{10}O_2$	102	102
12		$C_2H_4NaO_2^+$	83	83

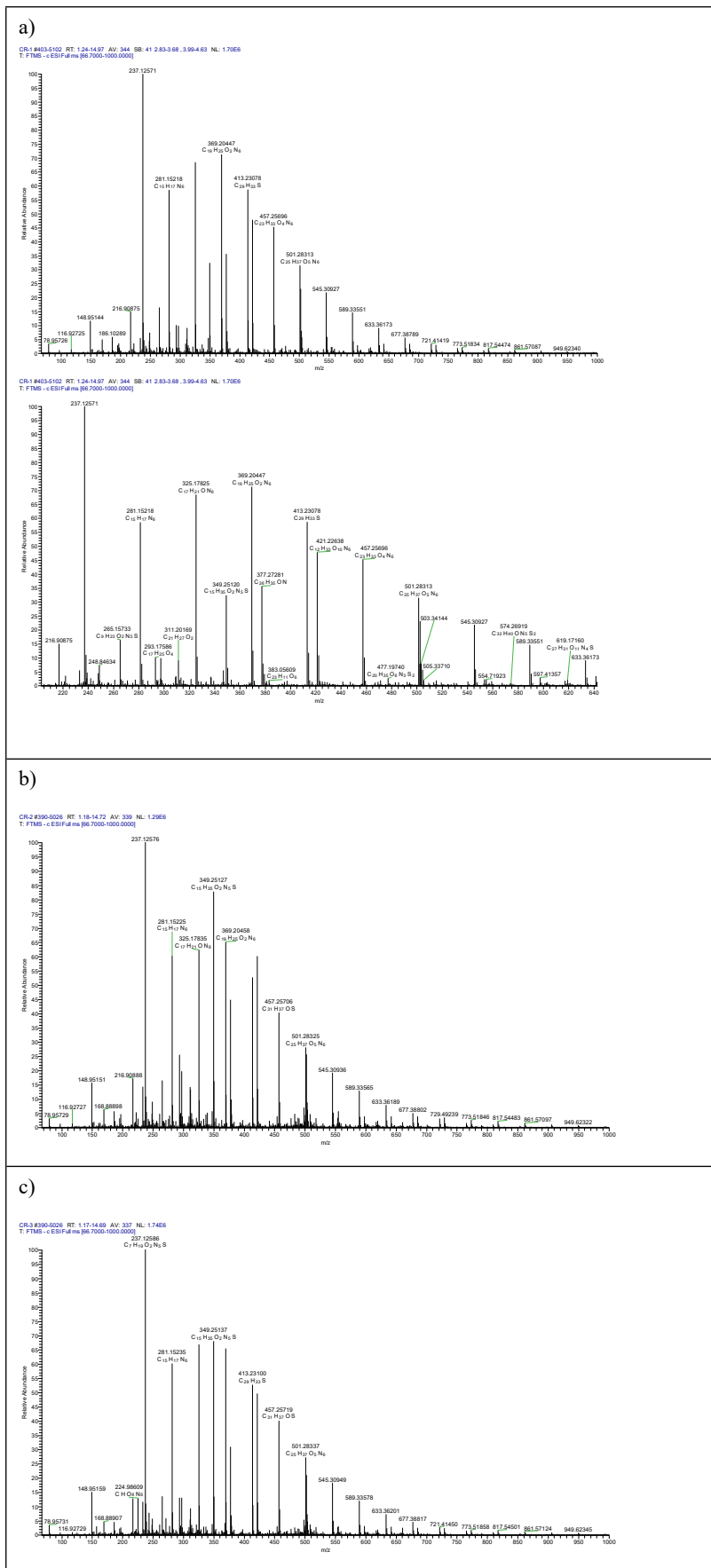
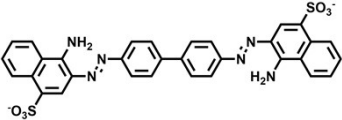
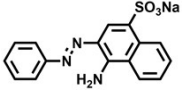
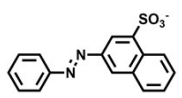
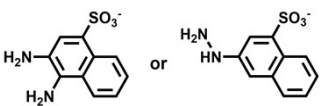
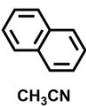
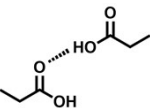
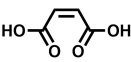
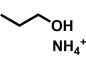


Fig. S10. The MS spectra of the photodegradation products of CR at different photodegradation times: (a) 5 min, (b) 15 min, and (c) 40 min.

Table S6. Detected intermediates of CR degradation by 3Ph-CTF using HPLC-MS.

Compounds	Chemical structure	Molecular formula	m/z
CR		$C_{32}H_{22}N_6O_6S_2^{2-}$	650
1		$C_{16}H_{12}N_3NaO_3S$	349
2		$C_{16}H_{11}N_2O_3S^-$	311
3		$C_{10}H_9N_2O_3S^-$	237
4		$C_{12}H_{11}N$	168
5		$C_6H_{12}O_4$	148
6		$C_4H_4O_4$	116
7		$C_3H_{12}NO^+$	78

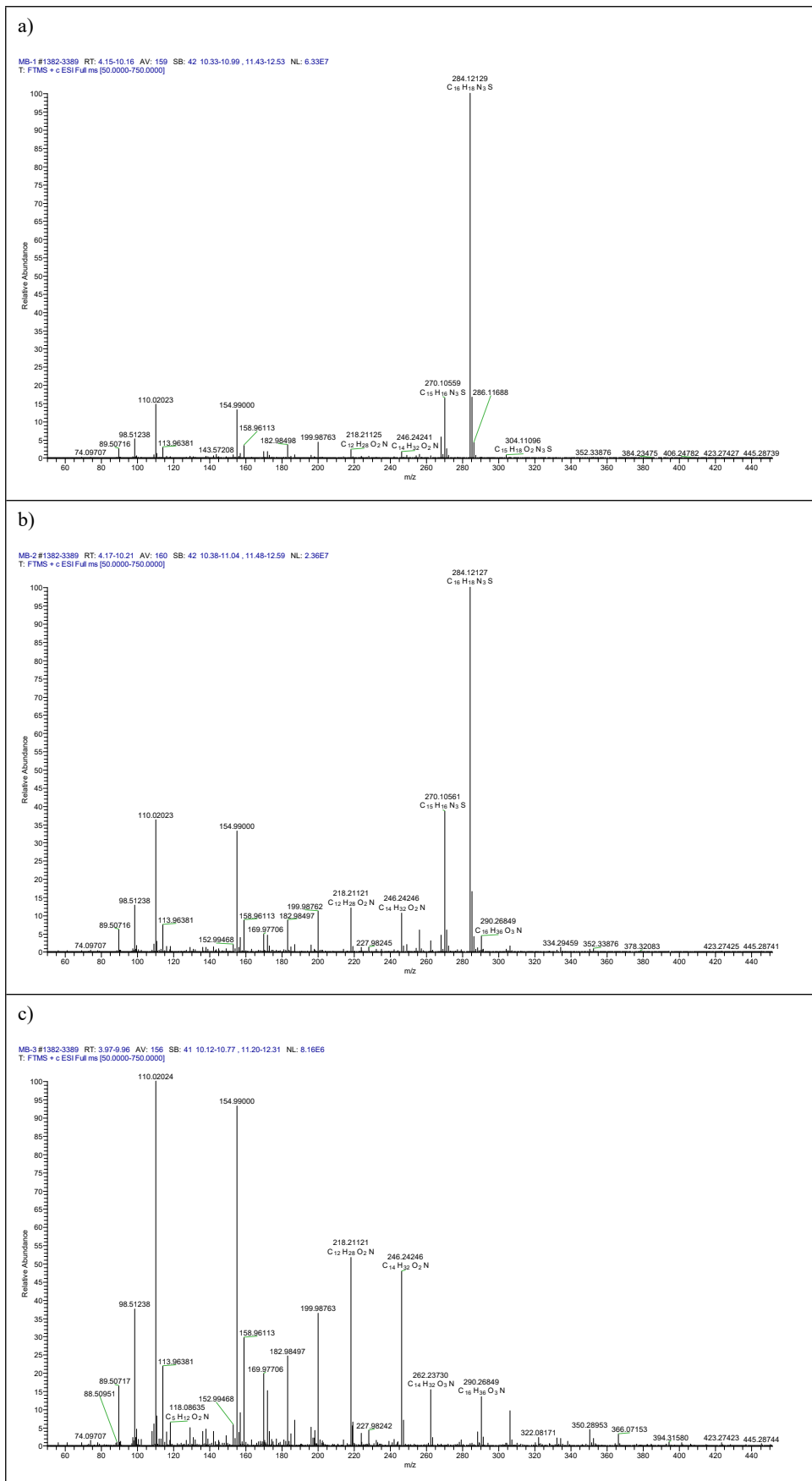
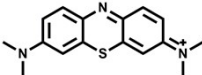
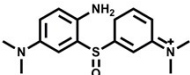
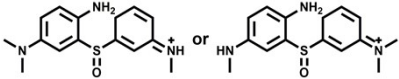
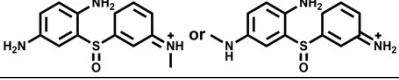
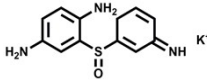
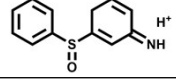
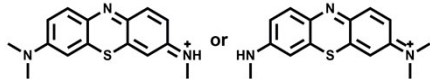
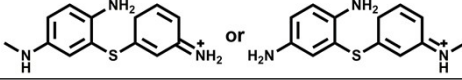
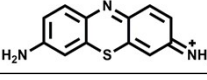
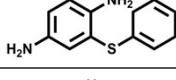
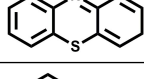
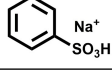
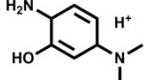
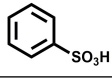
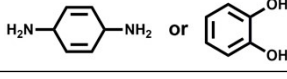
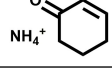
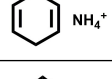
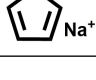
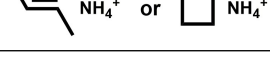


Fig. S11. The MS spectra of the photodegradation products of MB at different photodegradation times: (a) 25 min, (b) 60 min, and (c) 160 min.

Table S7. Detected intermediates of MB degradation by 3Ph-CTF using HPLC-MS.

Compounds	Chemical structure	Molecular formula	m/z
MB		$C_{16}H_{18}N_3S^+$	284
1		$C_{16}H_{22}N_3OS^+$	304
2		$C_{15}H_{20}N_3OS^+$	290
3		$C^{13}H^{16}N^3OS^+$	262
4		$C_{12}H_{13}KN_3OS^+$	286
5		$C_{12}H_{12}NOS^+$	218
6		$C_{15}H_{16}N_3S^+$	270
7		$C_{13}H_{16}N_3S^+$	246
8		$C_{12}H_{10}N_3S^+$	228
9		$C_{12}H_{14}N_2S$	218
10		$C_{12}H_9NS$	199
11		$C_6H_6NaO_3S^+$	182
12		$C_8H_{15}N_2O^+$	155
13		$C_6H_6O_3S$	158
14		$C_6H_{10}N_2$ $C_6H_6O_2$	110
15		$C_6H_{12}NO^+$	114
16		$C_6H_{12}N^+$	98
17		$C_5H_6Na^+$	89
18		$C_4H_{12}N^+$	74

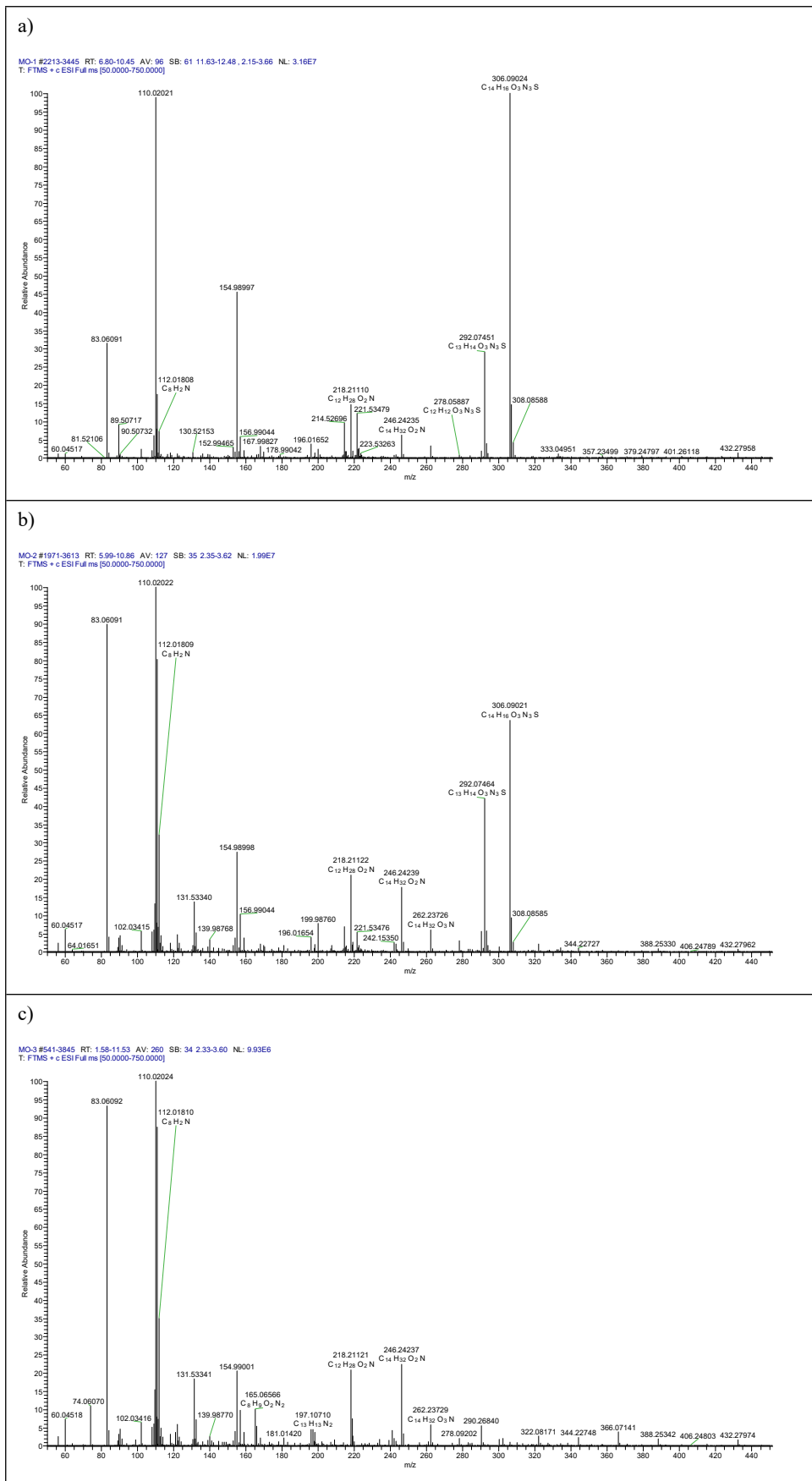
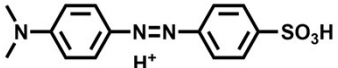
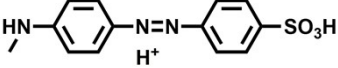
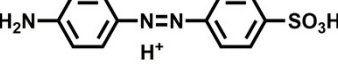
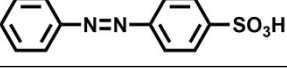
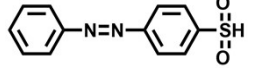
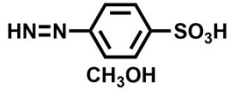
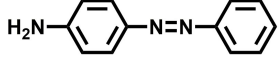
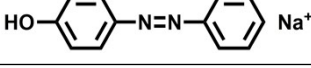
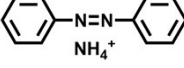
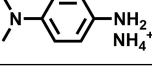
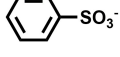
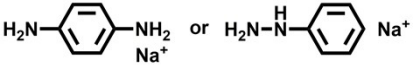

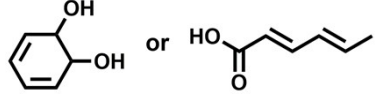
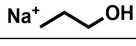
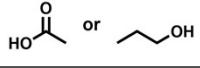
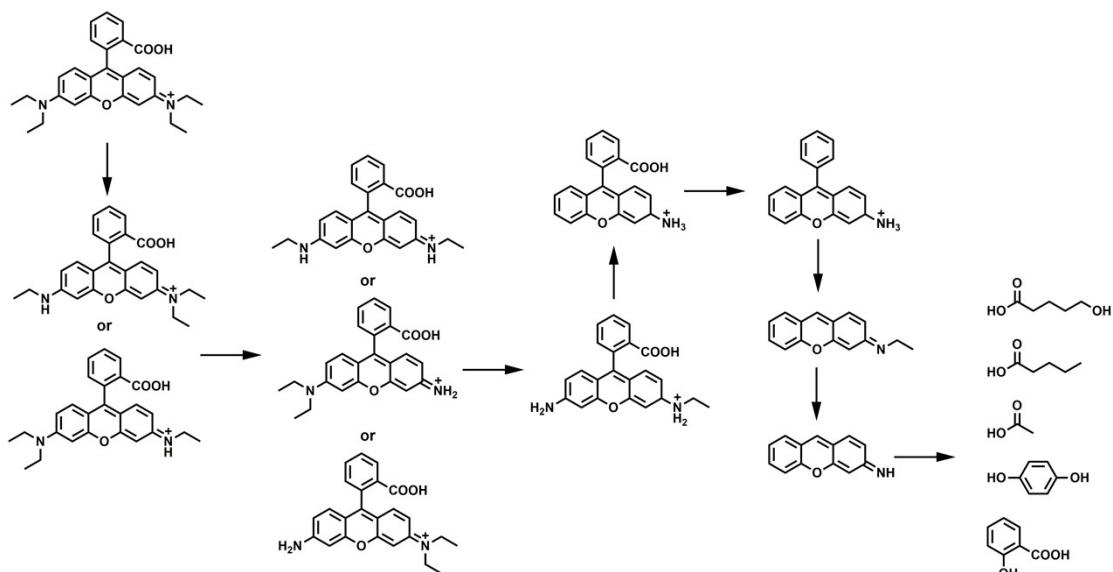


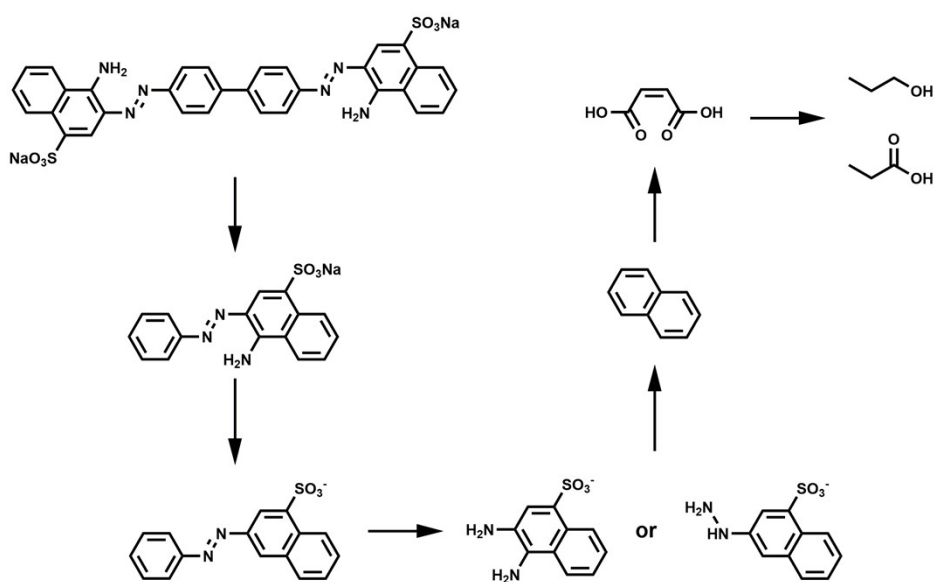
Fig. S12. The MS spectra of the photodegradation products of MO at different photodegradation times: (a) 40 min, (b) 70 min, and (c) 160 min.

Table S8. Detected intermediates of MO degradation by 3Ph-CTF using HPLC-MS.

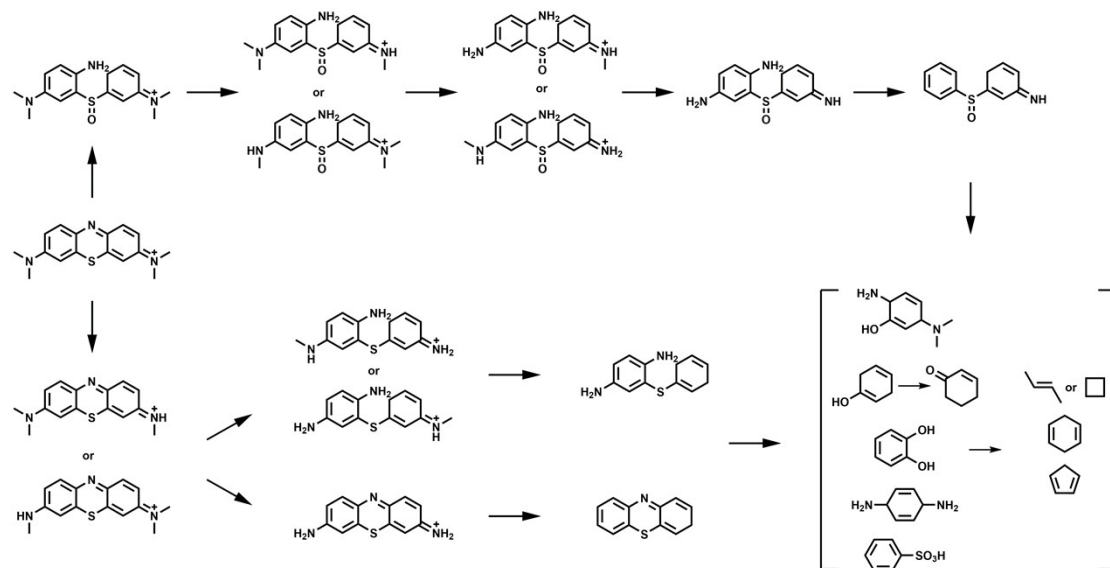
Compounds	Chemical structure	Molecular formula	m/z
MO		C ₁₄ H ₁₆ N ₃ O ₃ S ⁺	306
1		C ₁₃ H ₁₄ N ₃ O ₃ S ⁺	292
2		C ₁₂ H ₁₂ N ₃ O ₃ S ⁺	278
3		C ₁₂ H ₁₀ N ₂ O ₃ S	262
4		C ₁₂ H ₁₀ N ₂ O ₂ S	246
5		C ₇ H ₁₀ N ₂ O ₄ S	218
6		C ₁₂ H ₁₁ N ₃	197
7		C ₁₂ H ₁₀ N ₂ NaO ⁺	221
8		C ₁₂ H ₁₄ N ₃ ⁺	199
9		C ₈ H ₁₆ N ₃ ⁺	154
10		C ₆ H ₅ O ₃ S ⁻	157
11		C ₆ H ₈ N ₂ Na ⁺	131
12		C ₆ H ₆ O ₂	110
13		C ₆ H ₈ O ₂	112
14		C ₃ H ₈ NaO ⁺	83
15		C ₂ H ₄ O ₂ , C ₃ H ₈ O	60



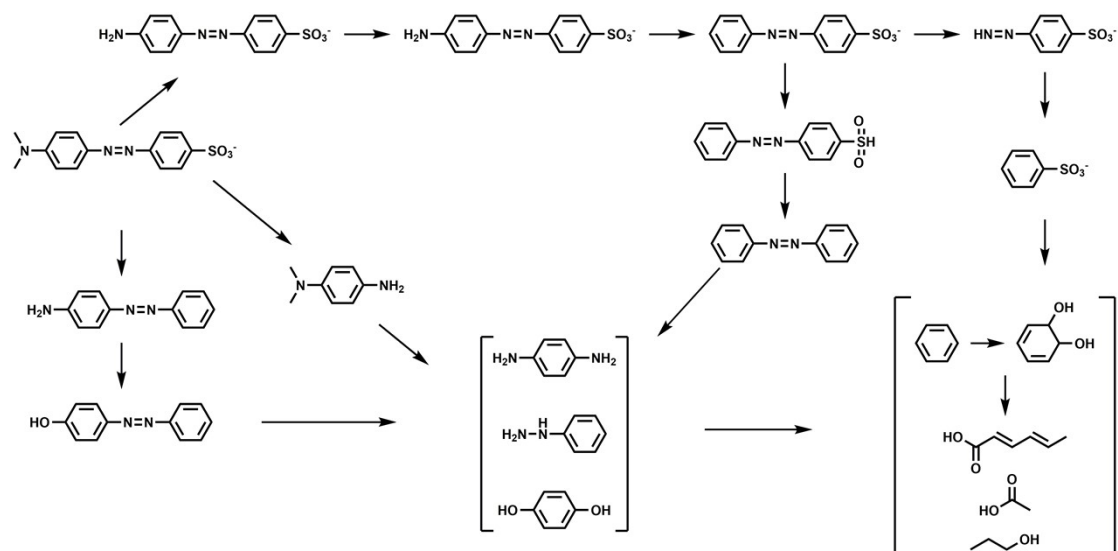
Scheme S1. Degradation pathway of RB by 3Ph-CTF based on degradation intermediates detected by LC-MS.



Scheme S2. Degradation pathway of CR by 3Ph-CTF based on degradation intermediates detected by LC-MS.



Scheme S3. Degradation pathway of MB by 3Ph-CTF based on degradation intermediates detected by LC-MS.



Scheme S4. Degradation pathway of MO by 3Ph-CTF based on degradation intermediates detected by LC-MS.

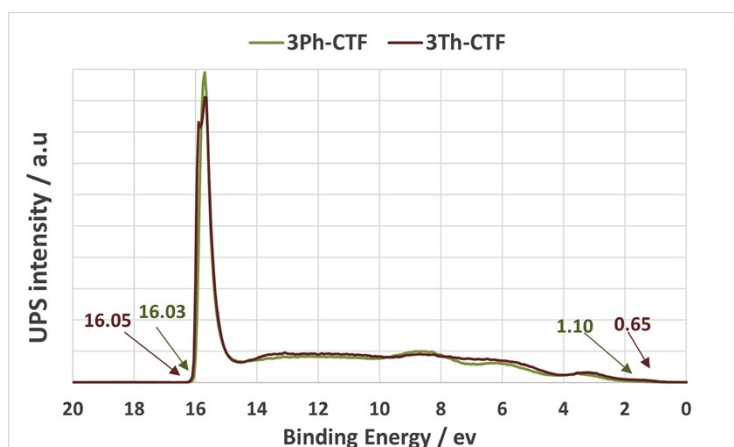


Fig. S13. Valence band UPS cutoff spectra of PTCTFs.

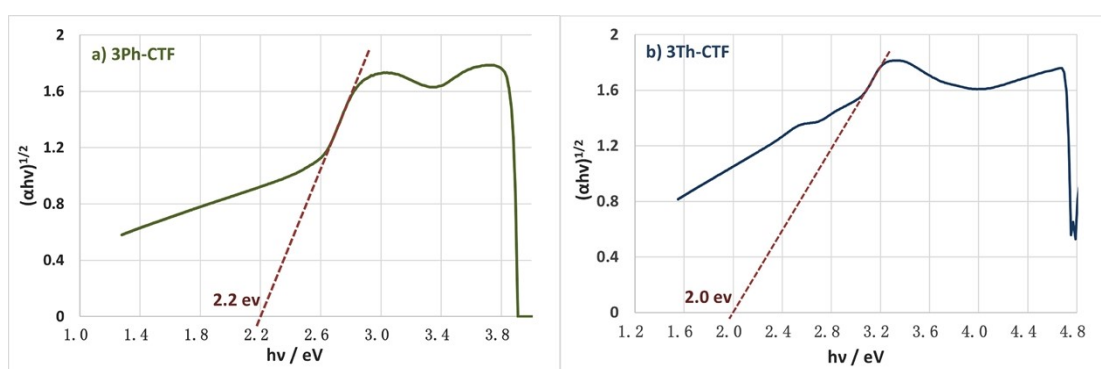


Fig. S14. The plots of $(\alpha hv)^{1/2}$ versus photon energy ($h\nu$) for CTFs.

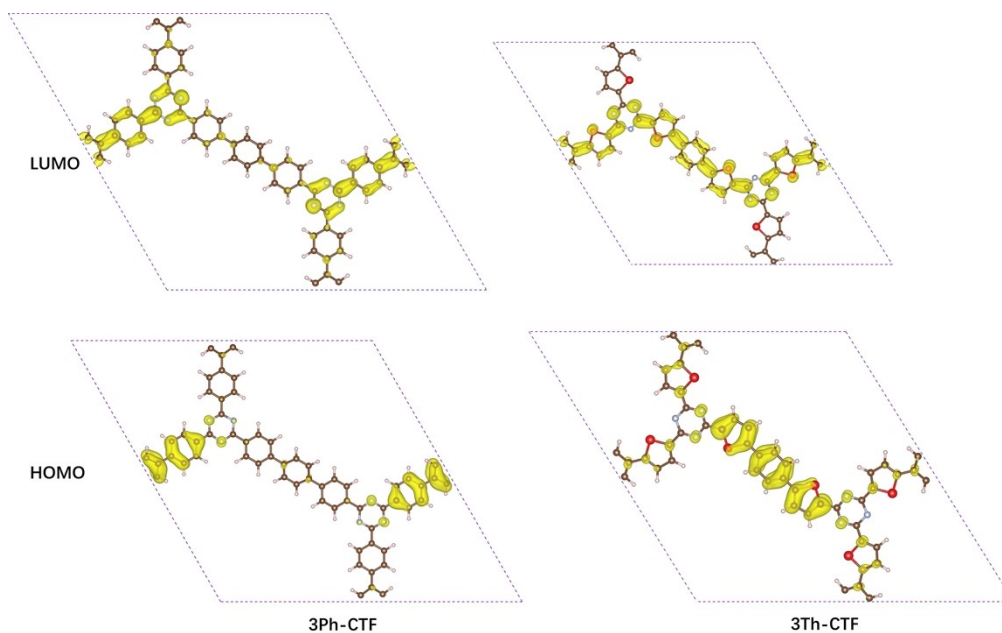


Fig. S15. The Kohn-Sham orbitals of HOMO and LUMO of CTFs.

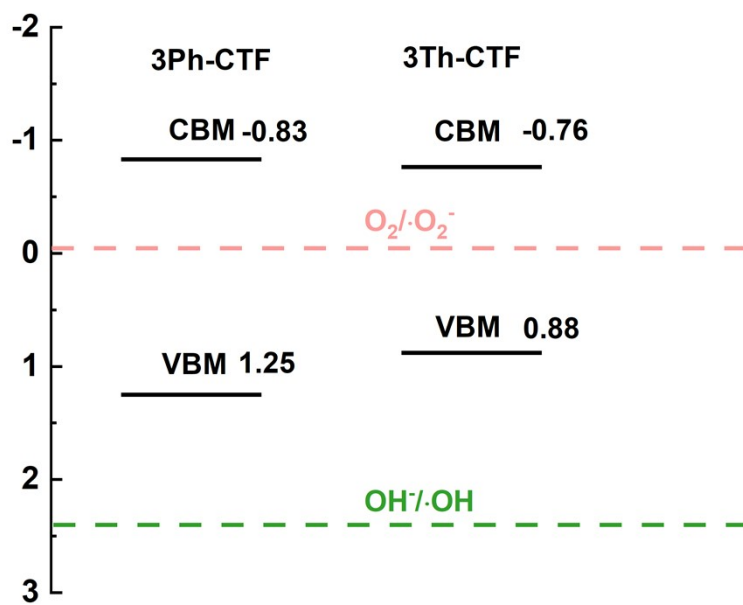


Fig. S16. The energy band structures of 3Ph-CTF and 3Th-CTF calculated by DFT.

REFERENCES

1. Kohn, W.; Sham, L. J., Self-Consistent Equations Including Exchange and Correlation Effects. *Phys. Rev.* **1965**, *140* (4A), A1133-A1138.
2. Kresse, G.; Furthmüller, J., Efficient iterative schemes for ab initio total-energy calculations using a plane-wave basis set. *Phys. Rev. B* **1996**, *54* (16), 11169.
3. Blöchl, P. E., Projector augmented-wave method. *Phys. Rev. B* **1994**, *50* (24), 17953-17979.
4. Perdew, J. P.; Burke, K.; Ernzerhof, M., Generalized gradient approximation made simple. *Phys. Rev. Lett.* **1996**, *77* (18), 3865.
5. Monkhorst, H. J.; Pack, J. D., Special points for Brillouin-zone integrations. *Phys. Rev. B* **1976**, *13* (12), 5188-5192.
6. Li, R.; Song, X.; Huang, Y.; Fang, Y.; Jia, M.; Ma, W., Visible-light photocatalytic degradation of azo dyes in water by Ag₃PO₄: An unusual dependency between adsorption and the degradation rate on pH value. *J. Mol. Catal. A: Chem.* **2016**, *421*, 57-65.
7. Shi, L.-L.; Zheng, T.-R.; Zhu, L.-M.; Li, K.; Li, B.-L.; Wu, B., A copper coordination polymer based on bis(imidazole) and thiophenedicarboxylate for photocatalytic degradation of organic dyes under visible light irradiation. *Inorg. Chem. Commun.* **2017**, *85*, 16-20.
8. Chaudhary, A.; Mohammad, A.; Mobin, S. M., Facile synthesis of phase pure ZnAl₂O₄ nanoparticles for effective photocatalytic degradation of organic dyes. *Mater. Sci. Eng., B* **2018**, *227*, 136-144.
9. Mahalingam, S.; Ramasamy, J.; Ahn, Y.-H., Enhanced Photocatalytic Degradation of Synthetic Dyes and Industrial Dye Wastewater by Hydrothermally Synthesized G-CuO-Co₃O₄ Hybrid Nanocomposites Under Visible Light Irradiation. *J. Cluster Sci.* **2018**, *29* (2), 235-250.
10. Liu, H.; Guo, W.; Li, Y.; He, S.; He, C., Photocatalytic degradation of sixteen organic dyes by TiO₂/WO₃-coated magnetic nanoparticles under simulated visible light and solar light. *J. Environ. Chem. Eng.* **2018**, *6* (1), 59-67.
11. Ran, X.; Duan, L.; Chen, X.; Yang, X., Photocatalytic degradation of organic dyes by the conjugated polymer poly(1,3,4-oxadiazole)s and its photocatalytic mechanism. *J. Mater. Sci.* **2018**, *53* (9), 7048-7059.
12. Sankar, M.; Jothibas, M.; Muthuvel, A.; Rajeshwari, A.; Jeyakumar, S. J., Structural, optical and Photocatalytic degradation of organic dyes by sol gel prepared Ni doped CdS nanoparticles. *Surf. Interfaces* **2020**, *21*, 100775.
13. Barman, D.; Paul, S.; Ghosh, S.; De, S. K., Cu₃N Nanocrystals Decorated with Au Nanoparticles for Photocatalytic Degradation of Organic Dyes. *ACS Appl. Nano Mater.* **2019**, *2* (8), 5009-5019.
14. Zhang, X.; Xia, M.; Wang, F.; Lei, W., Cu₂O/MoS₂ composites: a novel photocatalyst for photocatalytic degradation of organic dyes under visible light. *Ionics* **2020**, *26* (12), 6359-6369.
15. Nath, I.; Chakraborty, J.; Heynderickx, P. M.; Verpoort, F., Engineered synthesis of hierarchical porous organic polymers for visible light and natural sunlight induced rapid degradation of azo, thiazine and fluorescein based dyes in a unique mechanistic pathway. *Appl. Catal., B* **2018**, *227*, 102-113.
16. Xu, N.; Wang, R.-L.; Li, D.-P.; Meng, X.; Mu, J.-L.; Zhou, Z.-Y.; Su, Z.-M., A new triazine-based covalent organic polymer for efficient photodegradation of both acidic and basic dyes under visible light. *Dalton Trans.* **2018**, *47* (12), 4191-4197.